Received: 10 April 2019 | Revised: 10 October 2019 | Accepted: 3 November 2019

DOI: 10.1002/prot.25849

RESEARCH ARTICLE

PROTEINS WILEY

Molecular dynamics simulations to the bidirectional adhesion signaling pathway of integrin $\alpha_V\beta_3$

Martin Kulke | Walter Langel

Institut für Biochemie, Universität Greifswald, Greifswald, Germany

Correspondence
Walter Langel, Institut für Biochemie, Universität Greifswald, Felix-Hausdorff-Straße 4, 17487 Greifswald, Germany.
Email: langel@uni-greifswald.de

Peer Review
The peer review history for this article is available at https://publons.com/publon/10.1002/prot.25849.

Abstract

The bidirectional force transmission process of integrin through the cell membrane is still not well understood. Several possible mechanisms have been discussed in literature on the basis of experimental data, and in this study, we investigate these mechanisms by free and steered molecular dynamics simulations. For the first time, constant velocity pulling on the complete integrin molecule inside a dipalmitoylphosphatidylcholine membrane is conducted. From the results, the most likely mechanism for inside-out and outside-in signaling is the switchblade model with further separation of the transmembrane helices.

KEYWORDS
dihedral principal component analysis, extracellular matrix, membrane protein, steered molecular dynamics, talin

1 | INTRODUCTION

Integrin is a membrane protein of crucial importance in the adhesion complex of cells and transmits forces bidirectionally through the membrane. The two monomers integrin α_V and β_3 of the heterodimer consist of three main regions each—the extracellular domain outside the cell, the transmembrane part, which perforates the cell membrane, and the cytoplastic tails inside the cell. Integrins with several possible combinations of α- and β-chains are known,[1] and we focus here on $\alpha_V\beta_3$. Generally, the transport of adhesion signals by integrin from outside the cell to the inside and vice versa is not well understood. Therefore, in this study, the conformational changes and signal transmission for the outside-in activation resulting from an external force stimulus are investigated. By molecular mechanics, the response of only the extracellular domain to external forces has been traced.[2] Here, we develop a model for the full integrin structure and observed the change of the tertiary structure resulting from an applied force to the extracellular domain. The inside-out activation is studied by binding talin to closely connected and separated cytoplastic tail conformations and analyzing whether the presumably active and inactive transmembrane domain conformations give rise to switchblade movements in the extracellular domain.

1.1 | Outside-in activation mechanism

Outside-in activation is either mediated by binding of adhesion activators or by applying an external force to the cell. In the extracellular matrix, integrin molecules bind to fibronectin, collagen and more generally to the whole structural extracellular network, and an external force is not likely to act directly on a specific single integrin molecule,[3] but is transmitted simultaneously to several receptors. We mimic this by applying a weaker external force directly to the integrin head, to which the structural proteins are bound. Three possible activation pathways were discussed in literature for the outside-in activation so far:

Model 1: The simplest mechanism does not provide any substantial atomic displacements in the extracellular domain[4-7] (Figure 1, model 1). The forces only trigger slight shifts of some atomic groups being sufficient for enhancing the binding affinity of talin to the cytoplastic tail.

Model 2: The switchblade mechanism is more widely accepted, where the integrin extends by unbending of the knees near the head domain[8,9] (Figure 1, model 2).

Model 3: The third mechanism presumes a hinge like motion as described in (model 2) as a first step. In a second step, talin binds to only one of the two cytoplastic tails and the transmembrane helices

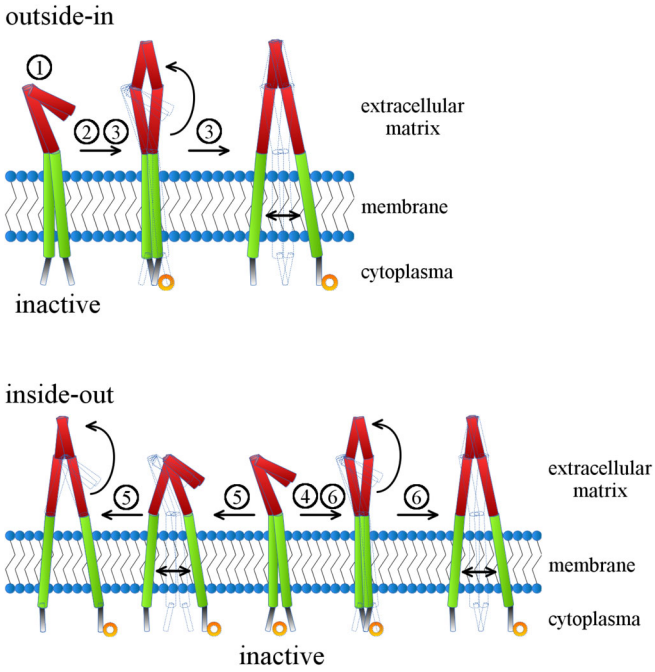

FIGURE 1 Schematic drawing of integrin structures according to different activation mechanisms (models 1-6) investigated in this study. The extracellular (*red*), transmembrane (*green*), and (*blue*) cytoplastic domains are indicated. Talin molecules are represented as orange circles

are separated by a force resulting from the motion of the actin cytoskeleton which is connected to talin[10-12] (Figure 1, model 3).

1.2 | Inside-out activation mechanism

The adhesion of integrin to other proteins in the extracellular matrix can also be triggered from inside the cell by binding of talin to the cytoplastic tails. For this inside-out activation, four models have been postulated that are related to the outside-in activation models:

Model 1b: The deadbolt model assumes that the β-tail domain acts as a lock for the adhesion site in the βA domain. Interactions of talin with the cytoplastic tails can then induce slight shifts in the β-tail domain that make the adhesion site accessible.[7,13,14]

Model 4: In the fourth model, talin binds to one or both cytoplastic tails and initiates the activation by pulling them together until they interact with each other or disrupting them.[15,16] This leads to a rearrangement of atomic groups in the transmembrane and the extracellular domain and ultimately integrin opens in a switchblade-like motion (Figure 1, model 4).

Model 5: The fifth possible mechanism is that talin binds specifically to the cytoplastic tail of the β-chain only. Then, the actin cytoskeleton connects to talin and pulls the transmembrane helical domains apart, which initiates the opening of integrin[17] (Figure 1, model 5).

Model 6: The sixth model is a combination of (model 4) and (model 5). In a first step, integrin is unbent as in (model 4) and in a second step the transmembrane helices are separated as in (model 5)[11,12,18] (Figure 1, model 6).

1.3 | Dihedral angle principle component analysis of simulated conformations

Protein conformational states are commonly characterized by reaction coordinates such as radius of gyration, number of hydrogen bonds, principle component analysis (PCA), end-to-end distance, solvent accessible surface area, and root mean square displacements, and often two coordinates have to be combined for specifically denoting conformations. In this study, dihedral PCA (dPCA)[19] is used to identify the conformation, describing the protein with internal backbone dihedrals φ_i and ψ_i, instead of using atomic coordinates as in standard PCA. This transformation greatly reduces the degrees of freedom and is not affected by translational or rotational overall motions of the protein.

2 | METHODS

2.1 | The integrin model

A complete model of the integrin $\alpha_V\beta_3$ was assembled for the first time combining various experimental results on its components. The large extracellular domain structure outside the cell was taken from the X-ray studies (PDB-code: 4G1E).[20] This domain has two parts, one with predominant α-helix and one with β-sheet structures. The α_V and β_3 subunits with five and eight modules, respectively, are bent at knees between the integrin headpiece and lower legs. The headpiece has a closed low-affinity conformation with predominant α-helix structures. The remaining extracellular domains form β-sheet barrel-like structures. The transmembrane domain was modeled in homology to the transmembrane domain of integrin $\alpha_{IIb}\beta_3$ (PDB-code 2K9J) using the SWISS server.[21,22] After homology modeling, α_V was aligned to the α_{IIb} chain in the $\alpha_{IIb}\beta_3$ template and the resulting three-dimensional structure of the $\alpha_V\beta_3$ unit was finally connected to the extracellular domain by hand. Further short amino acid sequences, for which no secondary structures exist, were added by hand as random coils. This is justified by the assumption that these missing sequences were not resolved due to a high structural flexibility. Since the template α_{IIb} of the transmembrane domain is shorter than the α_V chain itself, the remaining part of α_V on the cytoplastic tail, 1027 to 1048, is also modeled as coil.

Glycosylations and phosphorylations were applied according to UniProt (P06756 and P05106, cf. Figure S1).[23] The partially glycosylated protein was solvated in explicit water and the negative charge of the biomolecule was compensated by 44 sodium counter ions. Six calcium ions were added: Five ions are located in the Tigh and β-propeller domains (1 and 4, respectively) providing structural stability.[24] The sixth Ca^{2+} binds to the metal-ion-dependent-adhesion side (MIDAS) in the βA-domain. Experiments have shown that this calcium does not activate integrin, especially if the ion sites adjacent to MIDAS and the synergistic metal ion-binding side are unoccupied.[24] Therefore, integrin is not activated by ions and we assume that only responses to the external force are observed. In a later step, the integrin was imbedded into a dipalmitoyl-phosphatidylcholine (DPPC) membrane.[25]

2.2 | Molecular dynamics simulation

All simulations were calculated with the software package GROMACS 5.1.[26,27] Standard amino acids of the protein were represented within the AMBER99SB-ildn force field[28,29] and the FFPTM force field was applied to phosphothreonine (PTR, 767) and phosphotyrosins (773 and 785).[30] The parameters for glycosylated *N*-linked asparagine as well as the carbohydrates (Figure S1) were taken from Glycam,[31] and water was represented by the TIP3P model.[32] Periodic boundary conditions were applied with the cell sizes according to Table 1. All bond lengths were constrained with the LINCS algorithm.[33] Coulomb interactions were treated by the particle mesh Ewald method[34] with a grid spacing of 0.12 nm. A switching function with switching point and cutoff of 0.8 and 1 nm, respectively, was used for the van der Waals interactions.

First, each simulation cell was subjected to a minimization with the steepest descent algorithm until all forces on the atoms were converged to values below 10 kJ/mol/nm (17 pN). Calculations were continued by molecular dynamics simulations applying a Verlet integrator to the equations of motion with a time step of 2 fs in NVT and NPT ensembles. During equilibration, the temperature was adjusted to 300 K separately for the protein and other cell content with a modified v-rescale thermostat,[35] which enhances velocity rescaling by an additional stochastic term and ensures a proper canonical ensemble. The cell sizes were adjusted by applying two independent Parrinello-Rahman piston barostats[36] separating the xy-plane from the z direction, both with coupling time constants of 12 ps. This permitted to maintain the membrane with little stress curvature while adjusting the water density essentially by the cell height. The membrane itself was built by multiplying an equilibrated DPPC[25] membrane unit cell in the xy-direction and solvating the system with water. After minimization, the system was equilibrated for 0.4 and 0.6 ns in an NVT and NPT ensemble, respectively. The minimized structure of integrin was integrated into the system using the GROMACS tool "gmx insert-molecules," which placed the molecule into the membrane and removed overlapping DPPC and water molecules. The resulting artificial gap in the membrane was closed during a followed 5 ns long equilibration. This initial system was then used for the constant velocity pulling and interaction studies by either adding additional water in the case of vertical pulling or enlarging and equilibrating the membrane for the horizontal pulling (Table 1).

In preparation for the vertical pulling, a 102.5 ns long simulation in a NPT ensemble was conducted and different conformations at the times of 2.5, 52.5, and 102.5 ns were chosen as starting structures (Table 1). Thereby, we assume that the structure of the extracellular domain after 2.5 ns is still related to the initial X-ray structure and the later two conformations correspond to the equilibrium ensemble (Figure S2).

For the constant velocity pulling, a harmonic potential was applied with a force constant of 50 kJ/mol/nm^2 (0.08 N/m) between the C_a atoms of the integrin head and the transmembrane domain with reference distances constantly moving with speeds of 2 or 0.1 nm/ns in vertical or horizontal directions, respectively. The vertical pulling speed was previously optimized by Reference 2 on the same X-ray structure of the extracellular integrin domain. The very small force constant in combination with moderate pulling speeds resulted in a smooth and soft opening of integrin. After pulling, the systems relaxed for several 100 ns during NPT runs (Table 1). For consecutive relaxation simulations exceeding 1 μs, hydrogen mass repartitioning to 4 a.m.u.[37] was applied, and the time step was increased to 7 fs.

The reverse process, the closing of integrin, was accelerated by pulling the extracellular and transmembrane domains reducing their distance. Again, a force constant of 0.08 N/m and a constant velocity of 2 nm/ns were applied for pulling the two domains relative to each other.

In the horizontal pulling simulations, the high viscosity of the membrane, as compared to water, was accounted for by drastically reducing the pulling speed from 2 to 0.1 nm/ns, thereby reducing the viscous friction on the integrin transmembrane domain. In fact, each of the two helices in the transmembrane domain is pulled by 0.05 nm/ns away from its starting point, increasing their mutual distance by 0.1 nm/ns. This velocity of 5×10^7 nm/s is still magnitudes

TABLE 1 Simulation details. Columns contain from left to right the cell volume C_S, the numbers of membrane building units N_M and of water molecules N_W, the times of equilibration t_E and of pulling or morphing, t_{Pu} or t_M, respectively, and the relaxation time t_R for each simulation run. The brackets refer to the configurations at the end of each stage as plotted in Figures 2 and 5 (s. below)

Simulation		C_S (nm^3)	N_M	N_W	t_E (ns)	t_{Pu}, t_M (ns)	t_R (ns)
Vertical pulling	1	16 × 17 × 46	1025	365 761	2.5 (A1)	8.6 (B1)	80 (C1) + 148[a] (D1)
	2	16 × 17 × 46	1025	365 761	52.5 (A2)	8.6 (B2)	200 (C2)
	3	16 × 17 × 46	1025	365 761	102.5 (A3)	9.7 (B3)	280 + 746[b] (C3, D3)
Horizontal pulling		67 × 17 × 40	4100	1 318 582	4 (A4)	200 (B4)	105.3 (C4)
Morphing: activation		16 × 17 × 46	1025	365 761	2.5 (A5)	20 (B5)	1400 + 1260[b] (C5)
Morphing: deactivation		16 × 17 × 46	1025	365 761	2.5 (A6)	20 (B6)	353 (C6)
Talin binding: activation		16 × 17 × 14	1025	83 449	10.8	–	5 × 100
Talin binding: inactivation		16 × 17 × 15	1025	86 292	4	–	5 × 100

Abbreviation: HMR, hydrogen mass repartitioning.

[a]Deactivation by pulling (s. text).

[b]HMR and a time step of 7 fs were used.

larger than the speeds of the cytoskeleton motion in the cell of about 130 nm/s,[38,39] but such low values are not accessible in current simulation times. All trajectories were visualized with VMD 1.9.3.[40]

2.3 | Dihedral PCA

The application of dPCA to peptides has been described in Reference 19. In Reference 41, we showed that the conformations of small to medium sized peptides are unambiguously described by the first two main components of dPCA. Still the use of a larger number of main components might enhance the precision of the conformational assignment, but for clarity, we limit the evaluation to the first two.

2.4 | Probabilities of interactions

The interaction probabilities were calculated with a homemade program, which counts contacts between two amino acid residues on two different molecules in a trajectory and normalizes the results with respect to the number of frames similar to the method described in Reference 42. A contact between these residues is counted, if any

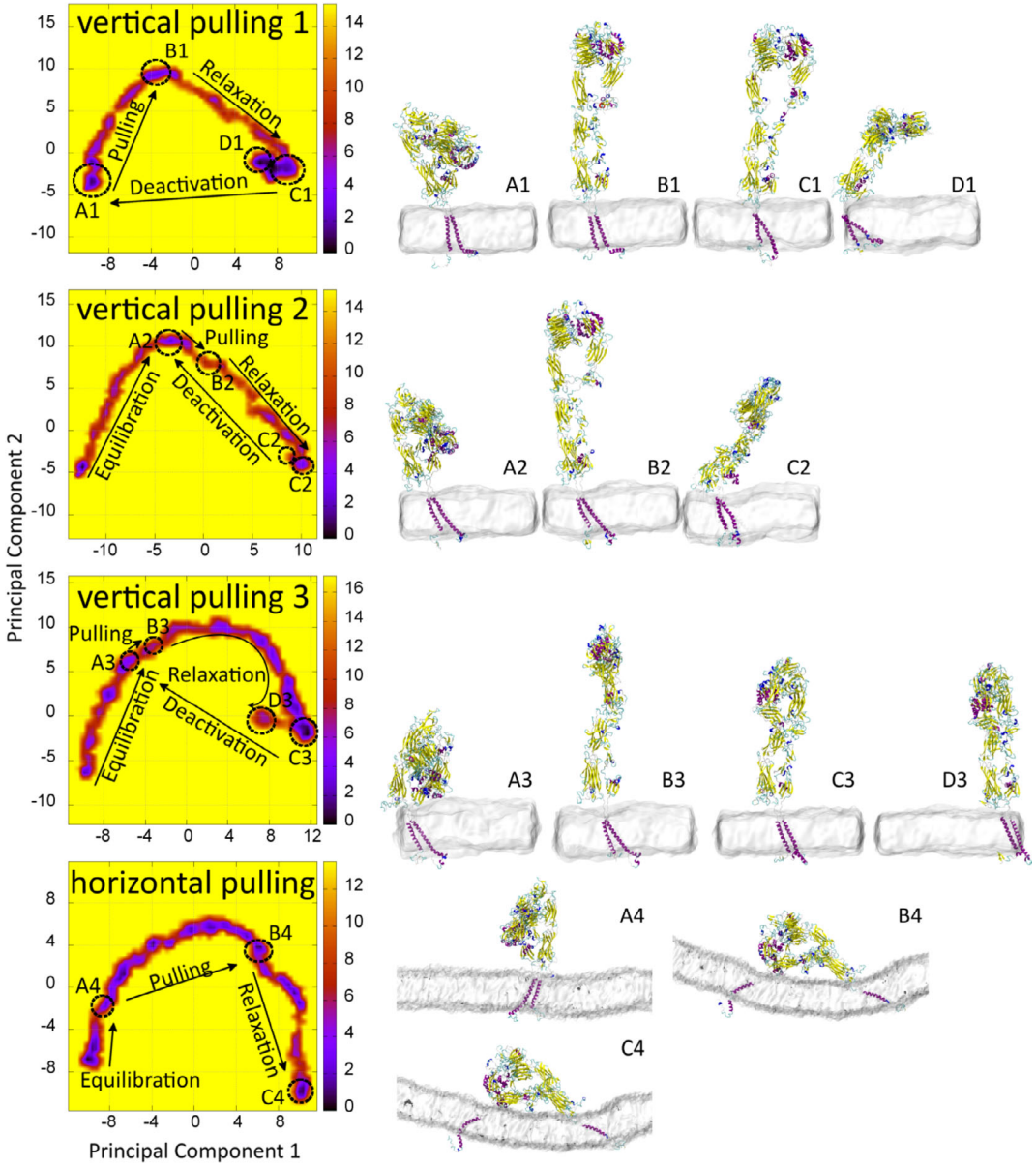

FIGURE 2 Outside-in activation with external forces applied in vertical (*top rows*) and horizontal (*bottom row*) directions. *Left column*: two-dimensional pseudocolorplots of the first two main components of the dihedral angle principle component analysis (dPCA) analysis. Areas with low and high free energies are indicated in *black* and *yellow*, respectively. The principal components in the four dPCA images are slightly different, and points with the same xy-coordinates may correspond to different conformations in different figures. *Right column*: Conformations of the integrin molecule corresponding to peaks **A1** to **C4** as indicated in the dPCA plots. The history for these conformations is given in Table 1 [Color figure can be viewed at wileyonlinelibrary.com]

atom on one of these two residues approaches any atom on the other one within 0.225 nm.

In our analysis, we group all residues of the same type on either protein. The resulting probabilities of binding may be greater than one, since each residue in one molecule may interact with more than one amino acid on the other one.

3 | RESULTS AND DISCUSSION

3.1 | Outside-in activation

3.1.1 | Steered molecular dynamics simulations

In Figure 2, the pulling pathways are visualized. The initial equilibration resulted in conformations **A**, and pulling started there. Structure **B** marks the final point of this pulling, where the stress was released. After relaxation without external stress, the protein attained the activated conformation **C**. In spite of the very different equilibration times before reaching state **A**, these final states of vertically pulling **C** differ only slightly in their conformation. Even though the main components were chosen independently for each dPCA plot, they are very similar. In all cases, vertical pulling at the integrin resulted in the unbending as prominent internal motion, which is well covered by the first main component of dPCA. It is more difficult to assign the second main component to a well-defined mode, but it could incorporate a breathing motion of the integrin.

During the vertical pulling of the integrin head (conformation **A** to **B**) the force first increases continuously but after around 10 nm of pulling pathway a significant barrier of about 400 pN is crossed and a drop of the force by about 100 pN is observed (Figure 3). With increasing equilibration time, this main peak is shifted to larger pulling distances.

Two effects contribute to this force during pulling vertically to the membrane:

1. The first contribution is the viscous force for pulling the large head through the water. If we assume that the Stokes law with the macroscopic viscosity of water also holds down to the microscopic dimensions of a peptide with a radius of gyration of the head group of 4.2 nm, we obtain a viscous force of about 150 pN at 2 m/s. This estimate is based on the spherical form of the head group. During a hinge motion, this group attains an extended structure and the friction will increase. We assign the continuously increasing component of the pulling force with increasing pulled distance of the virtual group to this effect (Figure 3A-C).
2. The second contribution arises from binding of the integrin βA-, hybrid, and PSI domains to the EGF1-4 and β-tail domains (Figure 4) with an energy of about 400 to 460 kJ/mol. This energy is composed of the dipole-dipole interaction of the βA-hybrid-PSI-domain dipole against the EGF1-4-β-Tail-domain dipole (calculated as 220-270 kJ/mol), two to three hydrogen-bridge bonds (Asn_{402} <-> Glu_{654}; Cys_{400} <-> Arg_{659}; Pro_{407} <-> Thr_{590}; 40-60 kJ/mol) and other contributions like van der Waals and quadrupole energies.

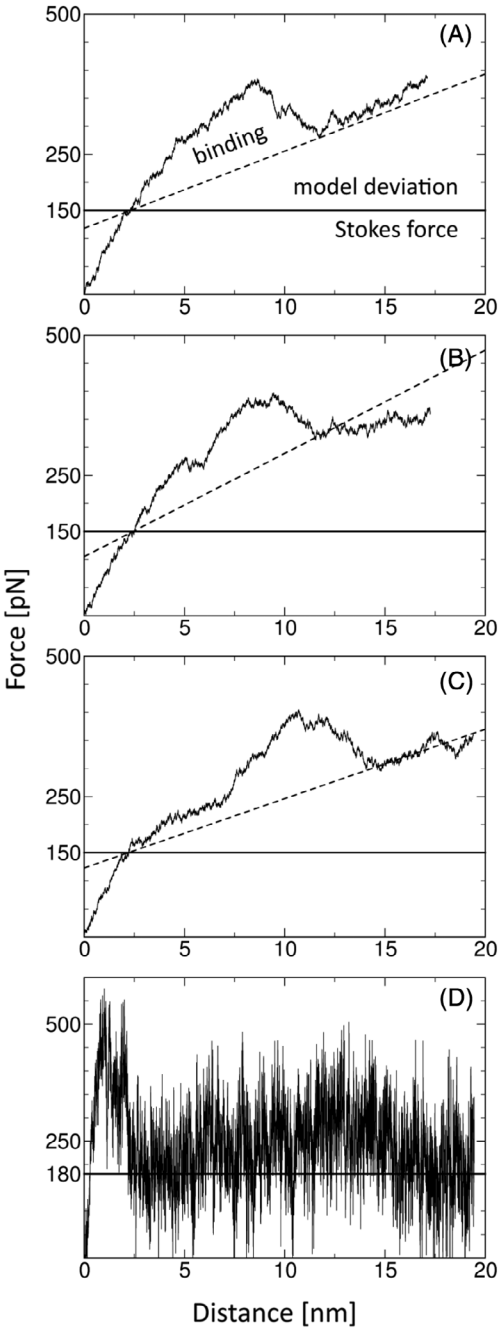

FIGURE 3 Force-distance curves for three vertical (A-C) and one horizontal (D) pulling simulations. The initial and final states of these curves are **A1**-**4** and **B1**-**4**, respectively (cf. Figure 2, *right column*)

3.1.2 | Torsion angle

In the inactive state, torsion angles between 25° and 35° are found (Table S1), which is consistent with the observation for the similar integrin $\alpha_{IIb}\beta_3$.[43,44] The vertically pulling in each of the three simulations resulted in a rapid decrease of the torsion angle between the transmembrane domains to less than 20° (Figure 5, *top row*, symbol **I** and Table S1). This event can occur directly during the pulling (Figure 5, *left*) or up to several 100 ns later (Figure 5, *right*). Then, 10 to 100 ns after this event, the angle recovers to around 20° to 24°,

and only after long relaxation times it further increased to the initial 25° to 35° (Figure 5, *right*). We assume that this recovery indicates the start of spontaneous deactivation.

3.1.3 | Tail-to-tail distance

During the initial relaxation, the two tails did not approach (Figure 5, bottom). Even after the long equilibration time of 100 ns, no contact between the two cytoplastic tails of α_V and β_3 was observed and their separation was about 1.5 nm in the inactive state.

After observing the decrease of the torsion angle between the transmembrane domains to less than 20°, the two tails approached within a delay of about 70 ns and reached a stably interconnected configuration (Figure 5, bottom, symbol **II**). This suggests that the closing of the cytoplasmic tails outside the cell is not incidental but correlated to the pulling of the ectoplasmic domain inside. We assume that unbending is a collective process involving rather complex motions beyond the change of the knee torsional angles only, and that the reduction of the tail-to-tail distances and torsional angles is correlated as parts of this motion. The final minimal end-to-end distance of 0.2 nm between the tails is determined by one to three unspecific hydrogen bonds. The most common case was the interaction of Arg1026 and Asn1042 with the phosphorylated amino acids Thr779 and Tyr785, but a short antiparallel sheet conformation with Thr777 <-> Glu1044 and Glu775 <-> Asn1046 was also observed.

We assign the close interconnection of the cytoplastic tails to the activation of integrin. The time for this activation event of integrin increases with increasing initial equilibration time. Presumably, this indicates that the initial X-ray structure is stressed and already in a semiactivated state. As integrin is a large protein, the relaxation from this initial stress takes several 100 ns (Figure 5, bottom row, Figure S2).

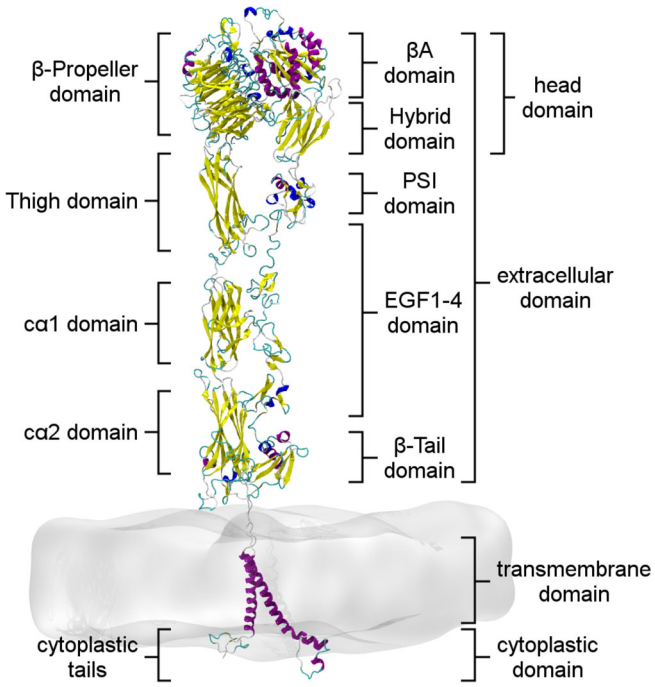

FIGURE 4 Naming for the integrin regions and domains. The metal-ion-dependent-adhesion side is located in the βA domain. The colors correspond to the secondary structure elements sheet (*yellow*), helix (*magenta*), 3-10-helix (*blue*), turn (*cyan*), and disordered (*white*) [Color figure can be viewed at wileyonlinelibrary.com]

3.1.4 | Deactivation as reverse process to activation

We tried to reverse the activation process and transfer the active state **C** as attained in the vertical pulling simulations back into the initial inactive conformation **A** in two different ways:

1. First, the deactivation was enforced by steered molecular dynamics after the vertical pulling simulation 1 (Figure 5, top row, left). The head group was pulled downward toward the

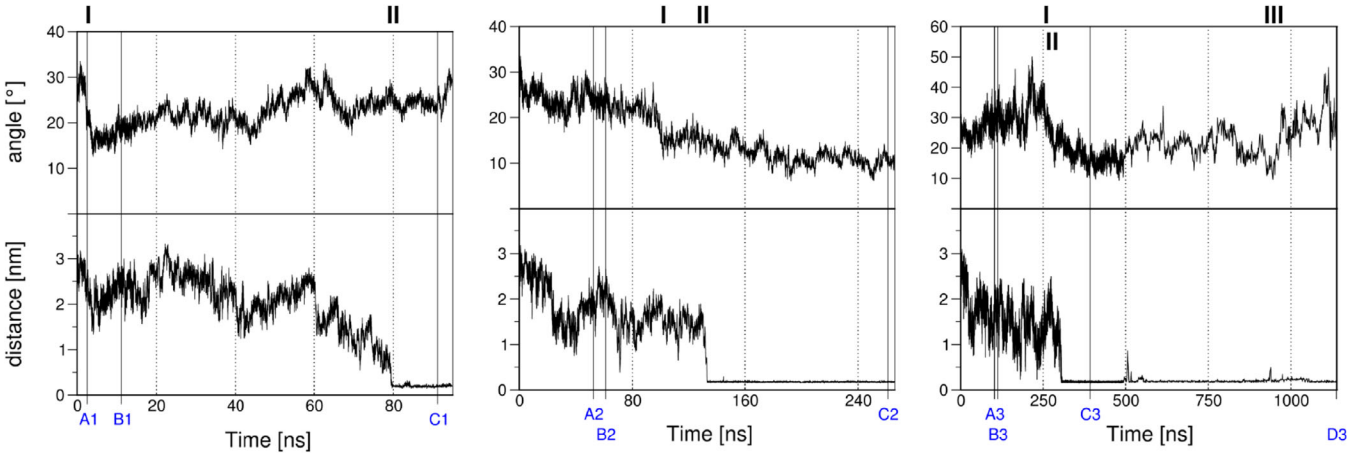

FIGURE 5 The torsion angle (*top*) between the main axes of the transmembrane helices between α_V and β_3 and the end-to-end (*bottom*) distance between the cytoplastic tails during the three vertical pulling simulations (*from left to right*: 1 to 3, with relaxation times 2.5, 52.5, and 102.5 ns, respectively) are plotted. The respective conformations are indicated (cf. Figure 2, *right column*). The symbols **I**, **II**, and **III** denote the drop of the torsion angle between the transmembrane helices, the approach of the cytoplastic tails and the increase of the torsion angle after long relaxation, respectively [Color figure can be viewed at wileyonlinelibrary.com]

transmembrane helices, but the inactive form could not be regained (Figure 2, top row).

2. To achieve spontaneous deactivation, the third vertical pulling simulation was continued by free molecular dynamics for about 1 μs. A trend toward the deactivated conformation **A** was revealed by the dPCA analysis (Figure 2, third row). The increase in the torsion angle of the transmembrane helices at around 0.9 μs (Figure 5, right, symbol **III**) could be a further indication of the start of deactivation. This indicates that the activated state is extraordinarily stable and the reverse process is very slow. We expect that the spontaneous deactivation will take a very long time and exceed the 1 μs simulation time by at least an order of magnitude. It is feasible from the cell point-of-view that the activation is a rapid response to the stimulus, but that the deactivation is much slower keeping the cell responsive for a significant time after the end of the stimulation.[7]

3.2 | Inside-out activation

3.2.1 | Horizontal pulling

The pathway of inside-out activation was analyzed by a horizontal pulling simulation. Here, the integrin displaces inside the highly viscous membrane. Pulling in a direction in the membrane plane ("horizontally") results in a completely different force distance curve (Figure 5D), and the contributions to the force are probably very different:

1. We assume that at the start the protein has to overcome a high energy barrier, since the lipid network is rather rigid and the intermolecular Coulomb and van der Waals interactions between the two helices in the transmembrane domain are strong.
2. The transmembrane helices then are pulled through regions of medium and high viscosity leading to a strong fluctuation in the plot. The average membrane resistance itself is about 180 pN as seen in the force distance curves after the initial high barrier (Figure 3). This corresponds to a lipid viscosity of 0.12 Pa/s for a spherical shape with 1.6 nm radius. Experimentally, lipid viscosities are between 0.03 and 1.5 Pa/s,[45] which is 30 to 1500 times higher than in water and could give rise to a force fluctuation between 45 and 2300 pN. We ascribe the noisy trace in Figure 5D to this effect.

The total force is much higher than during vertical pulling (Figures 2D and 3D) and acts on a smaller protein fragment. This high stress led to the destruction of the secondary structure of the

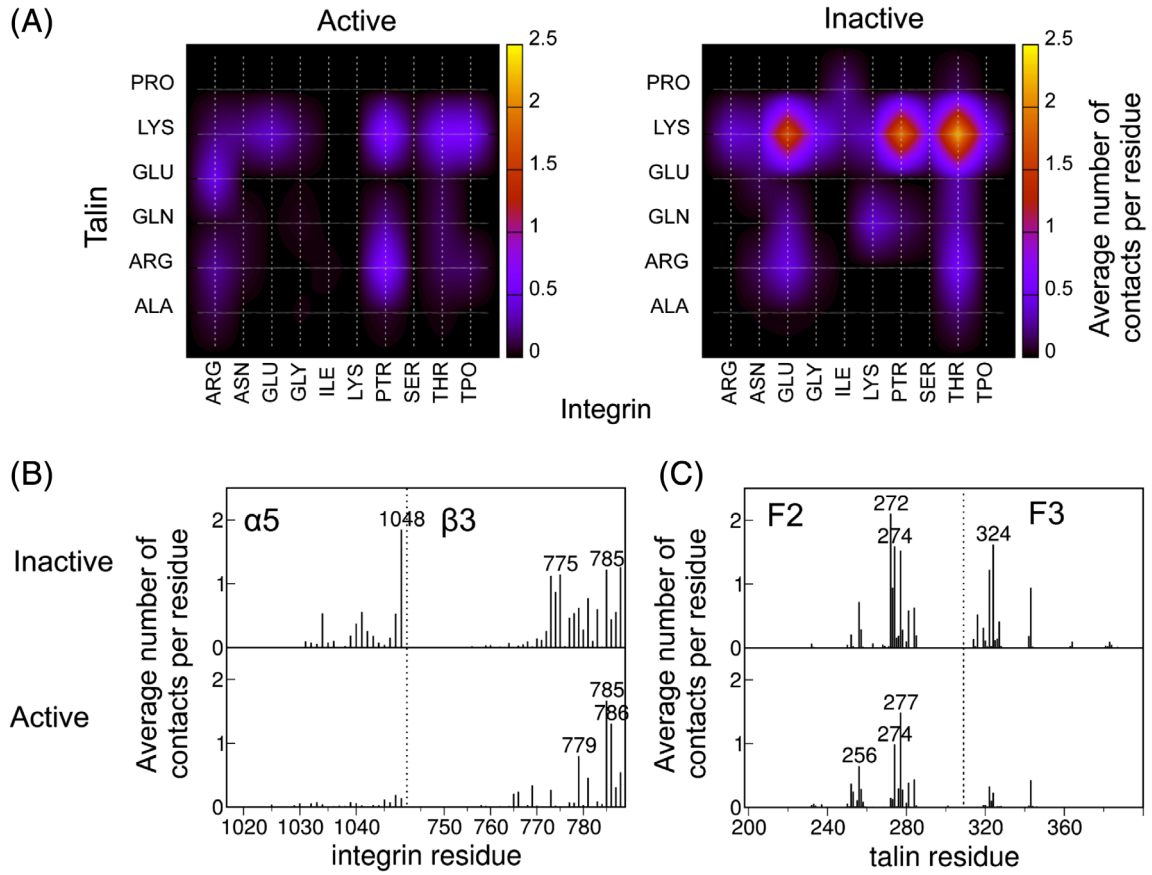

FIGURE 6 A, Interaction maps between amino acid species on integrin vs talin for the active (*left*) and inactive (*right*) cytoplastic tails conformations. Black and yellow colors indicate low and high interaction probabilities, respectively. The colors indicate that binding of talin to the inactive integrin is by roughly a factor of three more frequent than to the active molecule. B, Interaction probabilities between specified residues on integrin tails α_V (residues 1017-1048) and β_3 (residues 742-789) to the talin F2 (198-308) and F3 (309-400) domains. The abscissa denotes the integrin (*left*) and talin residues (*right*), respectively. Labels indicate the residues of the main interaction partners. The dotted vertical lines separate the interactions for the different domains [Color figure can be viewed at wileyonlinelibrary.com]

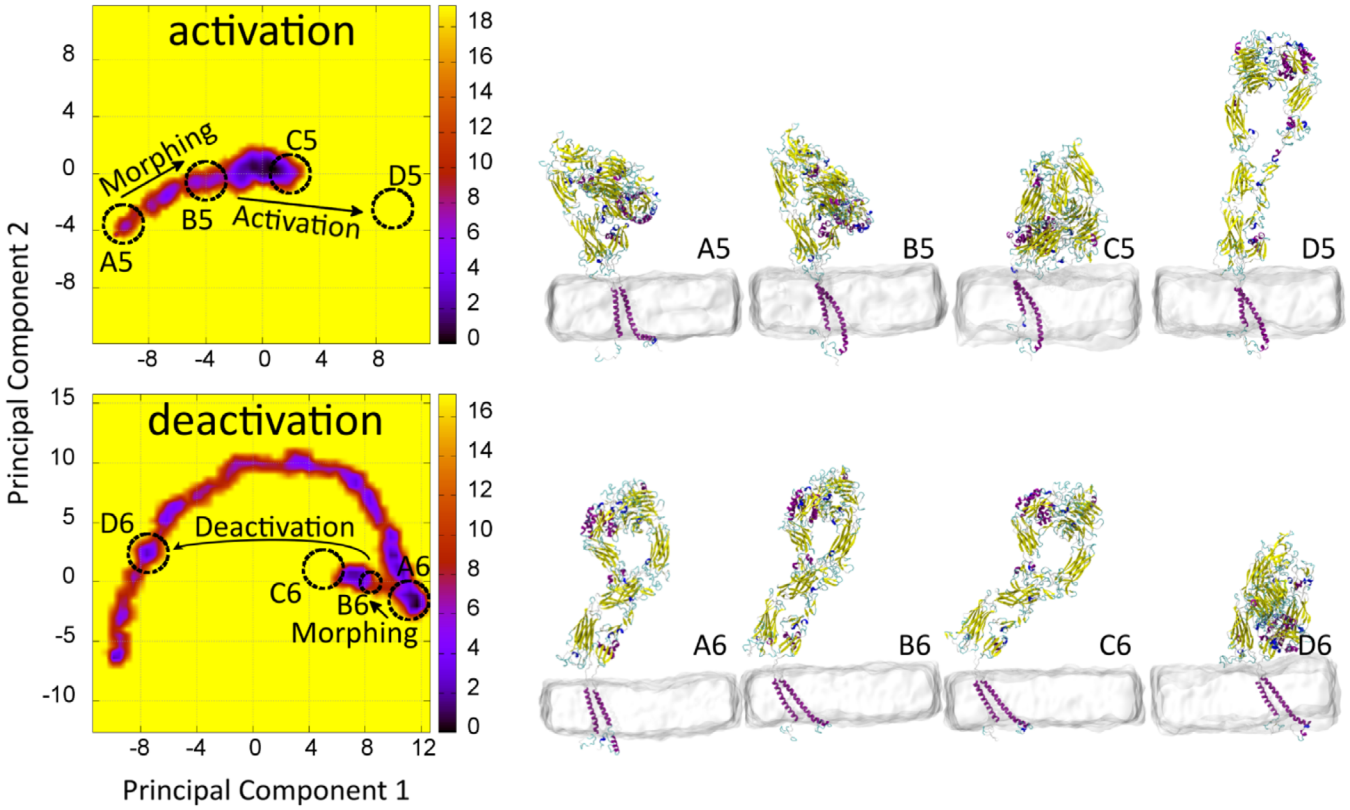

FIGURE 7 As Figure 2, but for inside-out activation (*top*) and deactivation (*bottom*). (*Left*) Dihedral angle principle component analysis (dPCA) plots and (*right*) the corresponding conformations for the peaks **A5** to **D6**. **A5** and **A6** are identical to **A1** and **C3**, respectively, while for the conformations **B5** and **B6**, only the cytoplastic tails and transmembrane domains are identical to those of the structures **C1** and **A3**, respectively (cf. Figure 2). The extracellular matrix domain has evolved freely during the morphing simulation [Color figure can be viewed at wileyonlinelibrary.com]

transmembrane domains during the pulling and no upward motion of the extracellular domain was observed. We presume that this is an artifact of the high pulling speed in the simulation. Inside the living cell a slower velocity of integrin inside the membrane results from the cytoskeleton motion (cf. Figure 1) and this may leave the transmembrane domains intact during the horizontal pulling (Figure 1, models 5 and 6).

3.2.2 | Talin binding behavior

In the living organism, the forces, which were artificially imposed here to the system by steered molecular dynamics, may arise from binding of talin inside the cell to the integrin cytoplastic tails, initiating the unbending and activation of the extracellular domain. We analyzed the binding of the talin domains F2 and F3 to these tails using the starting configurations of inactive (**A1**) and active (**C3**) integrin, respectively. In the inactive state both cytoplastic tails interact with the F2 and F3 domain of talin (Figure 6B,C), mainly with the PTR, threonine, glutamate and the C-terminal residues (Figure 6A). In the active state, integrin shows a weaker, but more specific interaction, and mainly the F2 domain of talin binds to the β_3-tail of integrin.

This binding pattern suggests the following inside-out mechanism: Binding of talin to both tails initiates unbending by the switchblade motion of the ectodomain. After the activation, talin switches to a specific binding to the β_3 cytoplastic domain, still being connected to the cytoskeleton. Its natural motion displaces talin and forces a separation of the transmembrane helices, keeping integrin in the activated state of model 6.

3.2.3 | Reaction of the extracellular domain to activation and deactivation

For the signal transfer from the cell inside to its outside, it is important that the activation of the cytoplastic tails transforms the extracellular domain conformation, probably by initiating a switchblade motion. We observed this reaction by morphing the transmembrane and cytoplastic domains within several ns either from the respective structures in inactive **A5** to active **C1** or active **A6** to inactive **A3** (Figure 7). During the simulation time, no major structural changes or motions were observed within the extracellular domain, but dPCA revealed trends for both processes toward the respective state of the extracellular domain (Figure 7).

4 | CONCLUSION

In this study, the question of the mechanism for integrin outside-in and inside-out signaling was tackled by molecular dynamics simulations on the full integrin structure. Several mechanisms that had been

described earlier[4-18] were examined for their feasibility (Figure 1). The best description of the observations provides a switchblade motion followed by a separation of the transmembrane helices (Figure 1, model 6). Based on molecular dynamics simulations, the same mechanism was suggested recently as the most likely one for the similar integrin $\alpha_{IIb}\beta_3$.[3] For the outside-in signaling, we demonstrated that by forcing this switchblade motion in the extracellular domain, the torsional angle between the transmembrane helices changes enforcing the contact between the previously separated cytoplastic tails (Figure 5). The same mechanism seems to apply for the inside-out signaling. Talin binds to both cytoplastic tails of the inactive integrin and presumably initiates an unbending of the extracellular domain (Figure 6). This then reduces the binding affinity of talin especially to α_V and make the protein interact with the β_3 cytoplastic tail of integrin only (Figure 6B), leading presumably to a separation of the transmembrane helices with the above explained mechanism.

Although the study provides promising results, they are based on a few assumptions and limitations. The integrin model was put together by hand from an extracellular X-ray structure, a homology model of the transmembrane domain and several assumed random coil structures of missing sequences. Since the transmembrane domain is entirely in α-helix conformation, the homology guess seems accurate. The remaining added sequences on the other hand might have a distinct secondary structure, which they may not have adopted during the equilibration. Also, the observables obtained during the pulling depend majorly on the used parameters. In this study, we considered the resulting conformation after the pulling (Figure 2, structures B1-B4) as independent from these parameters. Finally, even though the dPCA pictures indicate a lengthy deactivation process after the integrin activation (Figures 2 and 7), it is not clear if this process will spontaneously complete during a long enough simulation.

Nevertheless, the presented study provides valuable insights and a plausible explanation for the integrin activation process and hopefully encourages future experimental studies for verifying the proposed mechanism.

ACKNOWLEDGMENT

The authors thank the high performance computing clusters HLRN and BRAIN for providing computational resources.

ORCID

Martin Kulke https://orcid.org/0000-0002-2689-2428

REFERENCES

1. Hynes RO. Integrins: bidirectional, allosteric signaling machines. *Cell*. 2002;110(6):673-687.
2. Chen W, Lou J, Hsin J, Schulten K, Harvey SC, Zhu C. Molecular dynamics simulations of forced unbending of integrin αVβ3. *PLoS Comput Biol*. 2011;7(2):e1001086.
3. Mehrbod M, Trisno S, Mofrad MRK. On the activation of integrin αIIbβ3: outside-in and inside-out pathways. *Biophys J*. 2013;105(6):1304-1315.
4. Ulmer TS. Structural basis of transmembrane domain interactions in integrin signaling. *Cell Adh Migr*. 2010;4(2):243-248.
5. Xiong J-P, Stehle T, Diefenbach B, et al. Crystal structure of the extracellular segment of integrin αVβ3. *Science*. 2001;294(5541):339-345.
6. Xiong J-P. Crystal structure of the extracellular segment of integrin alpha Vbeta 3 in complex with an Arg-Gly-asp ligand. *Science*. 2002;296(5565):151-155.
7. Arnaout MA, Mahalingam B, Xiong J-P. Integrin structure, allostery, and bidirectional signaling. *Annu Rev Cell Dev Biol*. 2005;21(1):381-410.
8. Beglova N, Blacklow SC, Takagi J, Springer TA. Cysteine-rich module structure reveals a fulcrum for integrin rearrangement upon activation. *Nat Struct Biol*. 2002;9(4):282-287.
9. Wang L, Pan D, Yan Q, Song Y. Activation mechanisms of αVβ3 integrin by binding to fibronectin: a computational study. *Protein Sci*. 2017;26(6):1124-1137.
10. Kim M. Bidirectional transmembrane signaling by cytoplasmic domain separation in integrins. *Science*. 2003;301(5640):1720-1725.
11. Zhu J, Zhu J, Springer TA. Complete integrin headpiece opening in eight steps. *J Cell Biol*. 2013;201(7):1053-1068.
12. Shattil SJ, Kim C, Ginsberg MH. The final steps of integrin activation: the end game. *Nat Rev Mol Cell Biol*. 2010;11(4):288-300.
13. Xiong J-P. New insights into the structural basis of integrin activation. *Blood*. 2003;102(4):1155-1159.
14. Xiong JP, Mahalingham B, Alonso JL, et al. Crystal structure of the complete integrin αVβ3 ectodomain plus an α/β transmembrane fragment. *J Cell Biol*. 2009;186(4):589-600.
15. Shimaoka M, Takagi J, Springer TA. Conformational regulation of integrin structure and function. *Annu Rev Biophys Biomol Struct*. 2002;31(1):485-516.
16. Wegener KL, Partridge AW, Han J, et al. Structural basis of integrin activation by Talin. *Cell*. 2007;128(1):171-182.
17. Takagi J, Petre BM, Walz T, Springer TA. Global conformational rearrangements in integrin extracellular domains in outside-in and inside-out signaling. *Cell*. 2002;110(5):599-611.
18. Vinogradova O, Velyvis A, Velyviene A, et al. A structural mechanism of integrin AlphaIIbBeta3 "inside-out" activation as regulated by its cytoplasmic face. *Cell*. 2002;110(5):587-597.
19. Altis A, Nguyen PH, Hegger R, Stock G. Dihedral angle principal component analysis of molecular dynamics simulations. *J Chem Phys*. 2007;126(24):1-10.
20. Dong X, Mi LZ, Zhu J, et al. αvβ3 integrin crystal structures and their functional implications. *Biochemistry*. 2012;51(44):8814-8828.
21. Biasini M, Bienert S, Waterhouse A, et al. SWISS-MODEL: Modelling protein tertiary and quaternary structure using evolutionary information. *Nucleic Acids Res*. 2014;42(W1):252-258.
22. Lau T-L, Kim C, Ginsberg MH, Ulmer TS. The structure of the integrin αIIbβ3 transmembrane complex explains integrin transmembrane signalling. *EMBO J*. 2009;28(9):1351-1361.
23. The UniProt Consortium. UniProt: a hub for protein information. *Nucleic Acids Res*. 2015;43(D1):D204-D212.
24. Zhang K, Chen JF. The regulation of integrin function by divalent cations. *Cell Adh Migr*. 2012;6(1):20-29.
25. Jämbeck JPM, Lyubartsev AP. Derivation and systematic validation of a refined all-atom force field for phosphatidylcholine lipids. *J Phys Chem B*. 2012;116(10):3164-3179.
26. Pronk S, Páll S, Schulz R, et al. GROMACS 4.5: a high-throughput and highly parallel open source molecular simulation toolkit. *Bioinformatics*. 2013;29(7):845-854.
27. Hess B, Kutzner C, van der Spoel D, Lindahl E. GRGMACS 4: algorithms for highly efficient, load-balanced, and scalable molecular simulation. *J Chem Theory Comput*. 2008;4:435-447.
28. Lindorff-Larsen K, Piana S, Palmo K, et al. Improved side-chain torsion potentials for the Amber ff99SB protein force field. *Proteins Struct Funct Bioinform*. 2010;78(8):1950-1958.

29. Aliev AE, Kulke M, Khaneja HS, Chudasama V, Sheppard TD, Lanigan RM. Motional timescale predictions by molecular dynamics simulations: case study using proline and hydroxyproline sidechain dynamics. *Proteins Struct Funct Bioinform*. 2014;82(2):195-215.
30. Khoury GA, Thompson JP, Smadbeck J, Kieslich CA, Floudas CA. Forcefield_PTM: Ab initio charge and AMBER Forcefield parameters for frequently occurring post-translational modifications. *J Chem Theory Comput*. 2013;9(12):5653-5674.
31. Kirschner KN, Yongye AB, Tschampel SM, et al. GLYCAM06: a generalizable biomolecular force field. Carbohydrates. *J Comput Chem*. 2008;29(4):622-655.
32. Jorgensen WL, Chandrasekhar J, Madura JD, Impey RW, Klein ML. Comparison of simple potential functions for simulating liquid water. *J Chem Phys*. 1983;79(2):926-935.
33. Hess B, Bekker H, Berendsen HJC, Fraaije JGEM. LINCS: a linear constraint solver for molecular simulations. *J Comput Chem*. 1997;18(12):1463-1472.
34. Ewald PP. Die berechnung optischer und elektrostatischer gitterpotentiale. *Ann Phys*. 1921;369(3):253-287.
35. Bussi G, Donadio D, Parrinello M. Canonical sampling through velocity rescaling. *J Chem Phys*. 2007;126(1):014101.
36. Parrinello M, Rahman A. Polymorphic transitions in single crystals: a new molecular dynamics method. *J Appl Phys*. 1981;52(12):7182-7190.
37. Feenstra KA, Hess B, Berendsen HJC. Improving efficiency of large time-scale molecular dynamics simulations of hydrogen-rich systems. *J Comput Chem*. 1999;20(8):786-798.
38. Hu K, Ji L, Applegate KT, Danuser G, Waterman-Storer CM. Differential transmission of actin motion within focal adhesions. *Science*. 2007;315(5808):111-115.
39. Kaizuka Y, Douglass AD, Varma R, Dustin ML, Vale RD. Mechanisms for segregating T cell receptor and adhesion molecules during immunological synapse formation in Jurkat T cells. *Proc Natl Acad Sci U S A*. 2007;104(51):20296-20301.
40. Humphrey W, Dalke A, Schulten K. VMD - Visual molecular dynamics. *J Mol Graph*. 1996;14:33-38.
41. Kulke M, Geist N, Friedrichs W, Langel W. Molecular dynamics simulations on networks of heparin and collagen. *Proteins Struct Funct Bioinform*. 2017;85(6):1119-1130.
42. Deriu MA, Grasso G, Licandro G, et al. Investigation of the Josephin domain protein-protein interaction by molecular dynamics. *PLoS One*. 2014;9(9):e108677.
43. Berger BW, Kulp DW, Span LM, et al. Consensus motif for integrin transmembrane helix association. *Proc Natl Acad Sci U S A*. 2010;107(2):703-708.
44. Zhu J, Luo B-H, Barth P, Schonbrun J, Baker D, Springer TA. The structure of a receptor with two associating transmembrane domains on the cell surface: integrin αIIbβ3. *Mol Cell*. 2009;34(2):234-249.
45. Nojima Y, Iwata K. Viscosity heterogeneity inside lipid bilayers of single-component phosphatidylcholine liposomes observed with picosecond time-resolved fluorescence spectroscopy. *J Phys Chem B*. 2014;118(29):8631-8641.

SUPPORTING INFORMATION

Additional supporting information may be found online in the Supporting Information section at the end of this article.

How to cite this article: Kulke M, Langel W. Molecular dynamics simulations to the bidirectional adhesion signaling pathway of integrin $\alpha_V\beta_3$. *Proteins*. 2020;88:679–688. https://doi.org/10.1002/prot.25849